Journal of Structural Geology 31 (2009) 237–250

Contents lists available at ScienceDirect

Journal of Structural Geology

journal homepage: www.elsevier.com/locate/jsg

Fluid involvement in the active Helike normal Fault, Gulf of Corinth, Greece

Ioannis K. Koukouvelas*, Dimitris Papoulis

Department of Geology, University of Patras, 26 500 Patras, Greece

ARTICLE INFO

Article history:
Received 3 March 2008
Received in revised form
22 November 2008
Accepted 29 November 2008
Available online 13 December 2008

Keywords:
Clay minerals
Hydrothermal and meteoric fluids
Helike Fault
Gulf of Corinth
Greece

ABSTRACT

Rock fabric and mineralogical composition from the fault core and the unaffected protolith have been used to define the role of the segmented Helike Fault to fluid flow. Sixty samples were investigated by XRD, SEM observation and SEM-EDS microanalyses. Detrital smectite, calcite, and quartz represent the mineral assemblage at the crest of the footwall block in Foniskaria sampling site. In this site smectite is enriched at the rims of the fault core. All other sampling sites located at the base of the fault scarp are characterized by detrital and newly formed minerals. Detrital minerals include plagioclase, quartz, calcite and illite in Nikolaiika sampling site, and smectite, illite, kaolinite, quartz, calcite in Selinous sampling site. In the latter sampling site erionite and cerussite are newly formed minerals with erionite considered as the hydrothermal alteration product of fluids at 80–100 °C. At the eastern fault segment illite, quartz and calcite (T13 site) corresponds to detrital minerals. Mineralogy in the fault core reflects its high permeability to down-flowing meteoric water and weak hydrothermal alteration. The rock fabric suggests mineral alignment parallel to the fault plane. Mineralogy indicates that the Aigion, Helike and Pyrgaki Faults in the Gulf of Corinth host hydrothermal activity at shallow levels.

1. Introduction

Faults usually change, in a complex manner, the hydrologic properties of rocks over time and space, offering either conduits or barriers to fluid flow (Hubbert and Rubey, 1959; Chester et al., 1993; Caine et al., 1996; Matthäi et al., 1998; Aydin, 2000; Shipton and Cowie, 2001; Davatzes and Aydin, 2005). The study of fluid flow and solute transport in fractured rocks offer great potential to answer key questions of management of groundwater, petroleum, nuclear or toxic wastes and the geological sequestration of CO_2 (Sibson, 1996; Tsang and Neretnieks, 1998; Gautschi, 2000; Jourde et al., 2002; Agosta et al., 2007). In addition, understanding of fluid flow in active fault zones can answer key questions of earthquake physics and chemistry (Pili et al., 2002; Koch et al., 2003; Miller et al., 2004; Berg and Skar, 2005; Tanaka et al., 2007).

Since Hubbert and Rubey's (1959) pioneering work on the fluid pressure and the faults strength, many authors have demonstrated that fluids play a significant role during faulting (i.e., Segall and Rice, 1995, 2006; Sibson, 2000; Rice, 2006). At present it is commonly accepted that the crustal fluids play a critical role on the stress accumulation, hydrofracturing and faulting. The stress accumulation influences the permeability, the aperture in single conduits and the pore pressure (Hickman et al., 1995; Holness, 1997; Sibson, 2000, 2007). Furthermore, there are several lines of evidences for stepwise transport or discharge of deeply originated fluids to upper fluid reservoirs by episodic flow processes (Byerlee, 1993; Zoback and Harjes, 1997; Sibson, 2007). In Vogtland/NW Czech Republic, several lines of evidences suggest micro-seismicity accompanied by fluid-related anomalies of fluidal processes like deeply originated CO_2, radon anomalies, slug-flow process in fluid-filled discontinuities and fluid transport through single conduits in a fractured rock volume (Koch et al., 2003).

Although slip is localized within a relatively thin shear zone on the order of mm (e.g. Noda and Shimamoto, 2005), fluid flow through faults is commonly related with a much wider zone that is known as the damage zone (Davatzes and Aydin, 2005 and references therein). Faults in various tectonic settings are characterized by a fault core and a damage zone that grades outward into a relatively less deformed host rock (Chester et al., 1993). Fractures of the damage zone and the fault core itself are commonly filled with clays (Warr and Cox, 2001). The role of clays in faults is crucial in accommodating slip along faults in a plastic manner, or supporting laminar slip along with particle reorientation and their hydration–dehydration reactions that control exerted pressure in finger-like flow paths (Kahr et al., 1990; Tessier et al., 1998; Fitts and Brown, 1999; Sibson, 2007; Sulem et al., 2007). Clay minerals in fault zones can be correlated with four distinct phases (α, β, γ, δ) of the seismic cycle (Warr and Cox, 2001 and references cited therein). Clay mineral formation occurs during the phase (α) of the seismic cycle, which is characterized by elastic strain accumulation, and is

* Corresponding author.
E-mail address: iannis@upatras.gr (I.K. Koukouvelas).

0191-8141/$ – see front matter © 2008 Elsevier Ltd. All rights reserved.
doi:10.1016/j.jsg.2008.11.018

renewed during the phase (δ) of the seismic cycle when pressure drops and decelerating after-slip allows infiltration of hot fluids and clay mineral transformation. Phases (β) and (γ) are related with anelastic deformation and the main-shock rupture. Neither of these phases appears to be related with clay mineral formation (Warr and Cox, 2001).

In the present paper we analyze clay minerals from four sampling sites in the footwall of the active Helike normal Fault in the Gulf of Corinth, Greece. Our study concentrates on the excellently exposed footwall block of the fault and studies the evidence for fluid flow through the fault by using clay minerals. The sampled part of the Helike Fault is analyzed in a combined X-ray diffraction, scanning electron microscopy and microanalyses, and detailed structural analysis. In addition we evaluate data from published geological, palaeoseismological and seismic tomography studies in order to draw conclusions on the role of fluid in the faulting within the westernmost end of the Gulf of Corinth.

2. Faults within the westernmost end of the Gulf of Corinth

This study is concentrated within the Gulf of Corinth which is known as a key area for studying active normal faults (Koukouvelas and Roberts, 2007) (Fig. 1). The Gulf is characterized by surface rupturing earthquake events, and rapid divergence of the northern and southern coasts (Briole et al., 2000; Doutsos and Kokkalas, 2001; Burton et al., 2004; Koukouvelas et al., 2005; Gallousi and Koukouvelas, 2007).

A staircase of north-facing WNW-trending active normal faults, which are segmented along their strikes at the surface, are present on the southern flank of the Gulf of Corinth (Fig. 1). Three of them control either large sedimentary basins or the coast of the Gulf and are known as the Pyrgaki, Helike and Aigion Faults from south to the north (Koukouvelas and Doutsos, 1996; Koukouvelas, 1998; Moretti et al., 2003). The three faults are characterized by their changing dips with depth, including highly dipping planes close to the earth surface and shallowly dipping planes at depth (Doutsos and Poulimenos, 1992; Briole et al., 2000; Kokkalas et al., 2006; Micarelli et al., 2006). Both high and low angle portions of these faults are active, hosting moderate to strong earthquakes or current seismicity (Koukouvelas and Doutsos, 1996; Bernard et al., 1997, 2006; Koukouvelas et al., 2001; Pantosti et al., 2004; Zahradnik et al., 2004). Two hypotheses exist regarding the transition between the high to the low angle parts of the faults. The first suggests listric nature of the normal fault (Doutsos and Poulimenos, 1992; Rigo et al., 1996; Bernard et al., 2006). Alternatively, the existence of a low dipping zone composed of a series of small faults, located at the base of the brittle-crust, has been proposed (Hatzfeld et al., 2000). Fracture analysis along these three faults indicates that their damage zones scales with their displacement, while the width of the fault core remains stable. All faults appear to maintain secondary porosity as is highlighted by the circulation of meteoric water through the faults (Micarelli et al., 2003, 2006).

3. The Helike Fault

The Helike Fault was ruptured over the recent past by a series of five strong earthquakes (Koukouvelas et al., 2005). The Helike Fault with a 22-km-long trace length, and >2 mm/yr slip rate is a crustal scale structure (Pavlides et al., 2004); it is divided into western and eastern segments, 9 and 13 km long, respectively, both of which control a well developed relief at the fault scarp (Fig. 2). The best known earthquake that ruptured the Helike Fault trace is the 1861

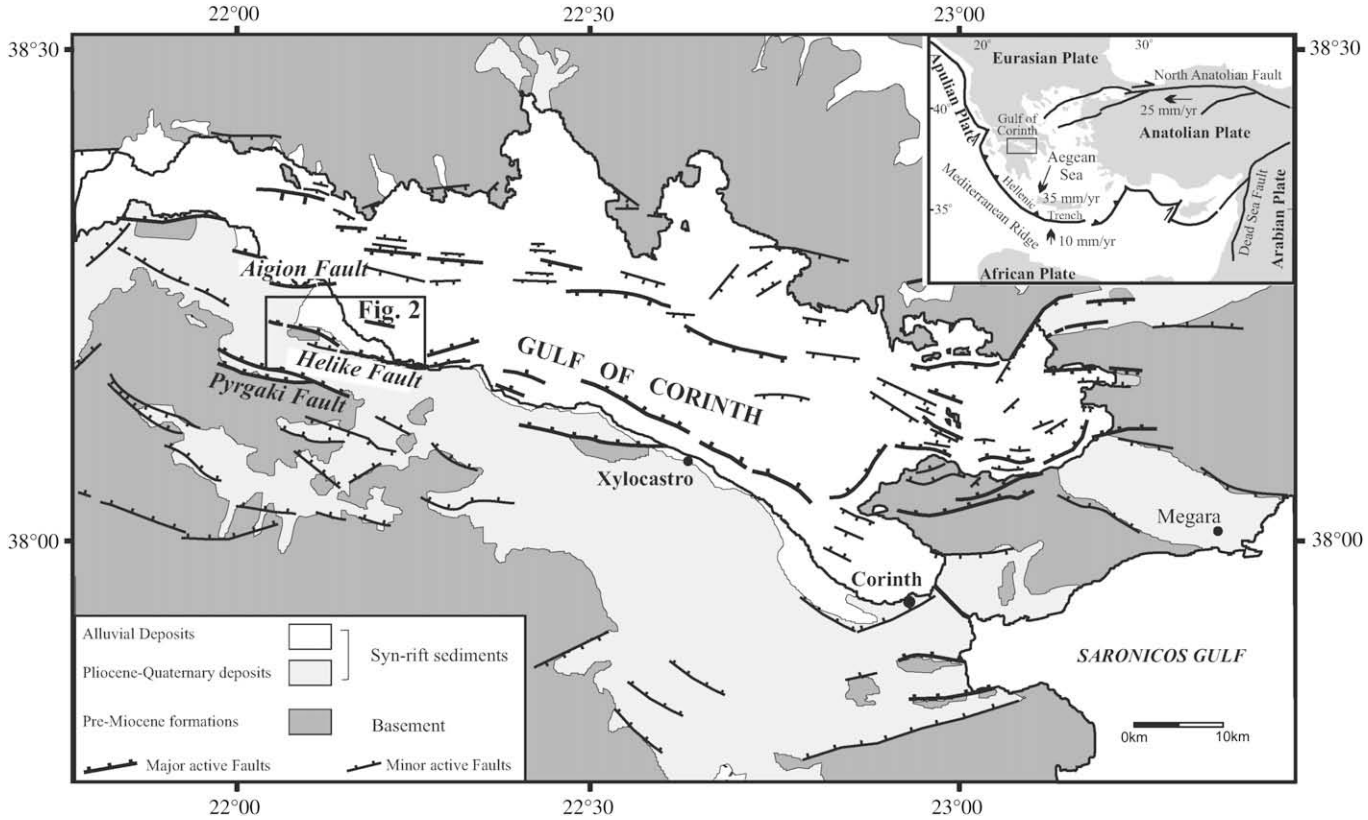

Fig. 1. Simplified structural map showing active normal faults within the Gulf of Corinth (simplified from Zygouri et al., 2008). Inset shows the location of the Gulf within the frame of lithospheric plates in the Eastern Mediterranean.

event ($M = 6.7$). This earthquake event happened during a period of anomalously high seismicity in the second half of the 19th century in the westernmost end of the Gulf of Corinth (Gallousi and Koukouvelas, 2007). Offset during the 1861 earthquake event was in the order of 1 m, a typical offset for the Helike Fault as well as for the entire Gulf of Corinth. Estimates based on trench tectonostratigraphy indicate that the minimum vertical displacement and extension accommodated by the East Helike Fault are as much as 1.5 and 1 mm/yr, respectively (Koukouvelas et al., 2001). The West Helike Fault segment juxtaposes Cretaceous limestone or Jurassic chert in its footwall, along more than 5.5 km of its length, while the east fault segment juxtaposes mainly Pliocene fan-deltas. The two fault segments are inferred to be linked at depth (Pavlides et al., 2004). Both fault segments include a series of parallel in trace second order parallel faults defining a fault damage zone in relation to the most important range-front fault (Koukouvelas et al., 2005). In the damage zone we consider as first order faults as those defining the range-front and hosting offset more than 300 m and as second order faults as those hosting offset up to 10 m and recognized within the Helike Fault damage zone. Our study is concentrated equally to the first and the second order faults.

The Helike Fault cuts at almost right angles a stack of Mesozoic nappes of the External Hellenides (Doutsos et al., 2006). The tectonostratigraphy of the External Hellenides is reviewed by Xypolias and Doutsos (2000), and comprises three units (from top to bottom): (a) the Triassic to Eocene age Pindos unit comprising deep-water carbonates, and siliciclastic and siliceous rocks. (b) The contemporaneous Tripolitsa unit comprising a thick carbonate sequence which is unconformably overlain by Oligocene to Miocene foredeep deposits. At its base Tripolitsa unit comprise the anchimetamorphosed Permian to upper Triassic age Tyros beds consisting of clastic and volcanic rocks. (c) The Permian–Middle Triassic aged Phyllite–Quartzite unit consisting of phyllites, schists and quartzites with local intercalation of metavolcanic rocks. The structural thickness of Hellenides is as much as 8 km (Doutsos et al., 2000, 2006). Seismic tomography data in the Aigion area suggests a two-layer vertical structure and the presence of a high Vp/Vs anomaly at depth interpreted as the effect of fluids on the rifting processes (Latorre et al., 2004). Magneto-telluric modeling suggests that the uppermost Pindos unit with an inferred thickness of 3 km is highly fractured (Pham et al., 2000). Temporary networks of seismographs suggest lack of current seismicity in the upper part of the crust down to 4 km depth (Bernard et al., 2006). The deeper part of the tomographic models is characterized by velocity increase suggesting the existence of the Phyllite–Quartzite unit at a depth greater than 5–7 km (Latorre et al., 2004). These low

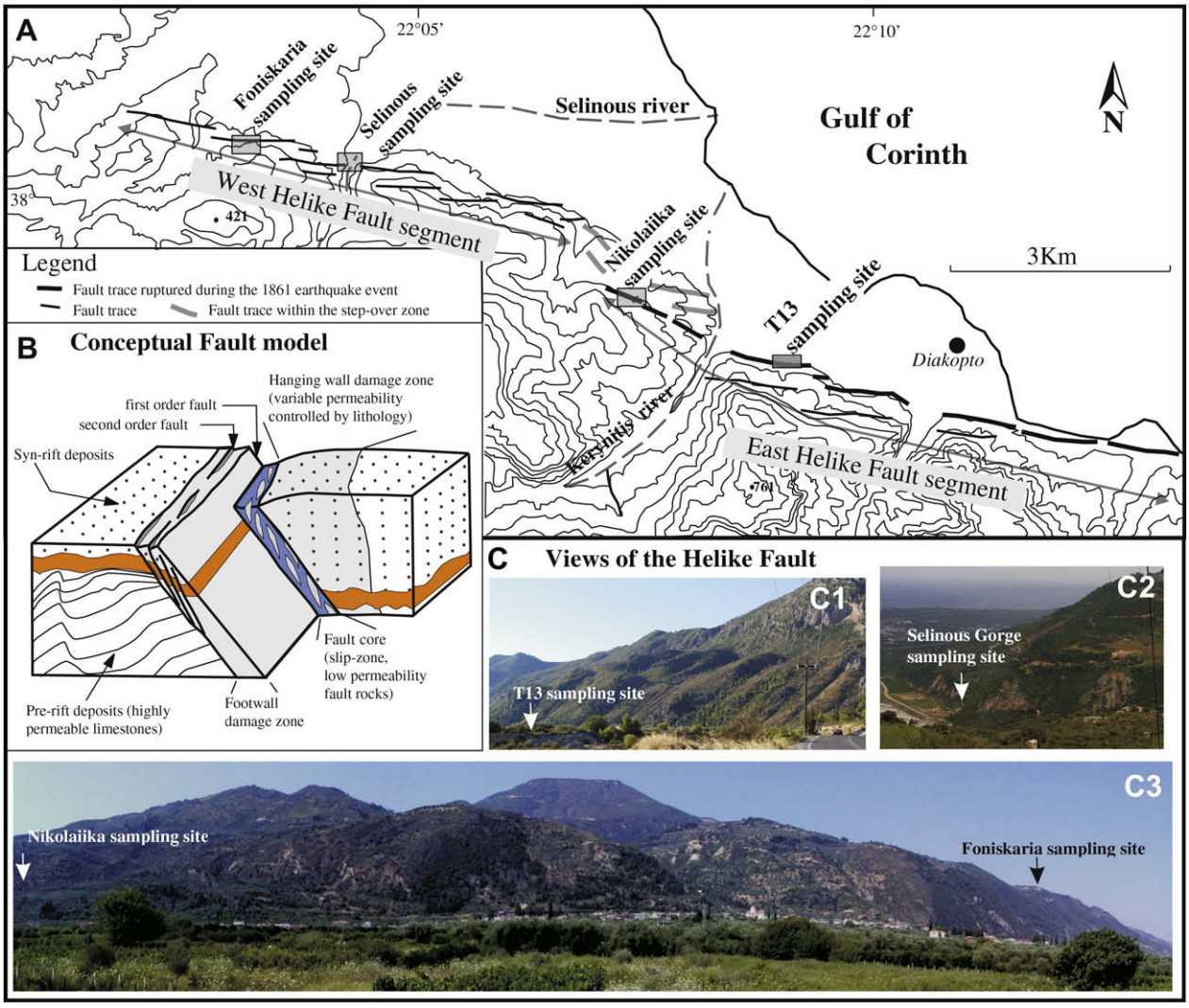

Fig. 2. (A) Structural map of the Helike Fault showing the prominent segments of the fault and sampling sites (modified from Pavlides et al., 2004). (B) A conceptual model for the Helike Fault; the diagram is schematic and not to scale. (C) Views of the Helike Fault showing the locations of the sampling sites.

velocity zones are parallel with the trend of the Gulf or large faults like the Helike Fault (Latorre et al., 2004).

4. Sampling strategy and analytical techniques

We studied four exposures that are structurally situated at the crest of the footwall and near the base of the relief developed by the Helike Fault. The analyzed samples were collected from 30 to 250 m long outcrops, oriented perpendicular to the fault zone. All sampling traverses start from the external margin of the fault core and cover the footwall damage zone and parts of the unaffected protolith within the footwall of the Helike Fault (Fig. 2). The footwall block is exposed at elevations from 40 to 410 m above sea level (asl) and since the fault dips at 55° north we sampled a structural depth of almost 500 m of the upper part of the fault.

Samples for this study were taken from both segments and all lithologies juxtaposed by the Helike Fault. Given that at depth the fault crosses the entire crust up to at least the depth of 9 km we suggest that possibly our sampling includes data for fluid flow representative for the upper part of the crust. The fault includes a series of second order faults defining a fault zone. The second order faults differ in number between the Pindos unit and the syn-rift sediments, being more abundant in the latter. In the syn-rift sediments we sampled both first and second order faults in the sampling sites of Foniskaria at 410 m, Nikolaiika at 110 m, and T13 at 40 m asl (Fig. 2). In the Selinous gorge sampling site at 70 m asl, where the fault juxtaposes Mesozoic limestones and Eocene flysch, we sampled only the first order fault that is exposed. Our sampling extended, where possible, across the 60–80 m wide damage zone of the fault as is described by Micarelli et al. (2003) (Fig. 2B).

Under this strategy, we collected 33 samples from the footwall rocks/protoliths and 27 samples from the fault cores. Our sampling strategy was focused on addressing three questions. (1) What is the distribution of clay minerals in the fault core and its surrounding rocks? (2) What is the role of clays in faulting, and do clays define barriers or conduits for fluid flow? (3) Is there any evidence for downward circulating meteoric waters or pumping back of deeply circulated fluids up to the surface?

All samples were analyzed using the following methods. Mineralogical compositions of bulk rocks and of the clay fractions (<2 μm), extracted by sedimentation, were determined by X-ray diffraction, using a Philips PW1050/25 diffractometer, with Ni-filtered, CuKα radiation. Oriented clay powders were prepared by the sedimentation method and were scanned at 1°2θ/min from 3 to 60°2θ. For each <2 μm specimen, clay minerals were identified from three XRD patterns (air-dried at 25 °C, ethylene–glycol solvated, and heated at 490 °C for 2 h). Quantitative estimates are based on modeled traces from NEWMOD © (Reynolds, 1985; Reynolds and Walker, 1993).

Smectite was identified by comparing diffraction patterns of air dried, ethylene–glycol solvated and heated preparations. The air dried preparation gives a strong 001 reflection at about 6°2θ (14.7 Å), which in the ethylene–glycol and heated preparations shifts to 5.2°2θ (16.9 Å) and 8.8°2θ (10.0 Å) respectively. The above procedure is the only way to discriminate smectite from chlorite and vermiculite using XRD. Special attention was given during the interpretation of the XRD patterns for the detection of mixed-layers illite–smectite. The existence of mixed layers highlights hydrothermal activity and/or possible shear heating within the fault core. Mixed-layer illite–smectite can be recognized from the XRD patterns of air-dried sample as a reflection at about 7.35°2θ (12 Å) which in the ethylene–glycol and heated preparations shifts to 6.8°2θ (13 Å) and 8.8°2θ (10.0 Å) respectively.

Mineral textures, morphology and chemical composition, for all 27 samples from the fault cores and nine samples from the footwall block, were determined using a JEOL 6300 scanning electron microscope (SEM) equipped with energy dispersive (ED) and wavelength dispersive (WD) spectrometers. The accelerating voltage was 15KV and the intensity data were corrected with a ZAF program. SEM photographs were obtained from gold coated fracture surfaces of bulk samples mounted on stubs and on epoxy resin-impregnated, polished and gold- or carbon-coated thin sections.

5. Analytical results

5.1. The mineralogy of the crest of the Helike Fault footwall (Foniskaria outcrop)

The Foniskaria outcrop, at an elevation of 410 m asl, is located at the crest of the footwall block corresponding to the upper tip of the fault, and near the middle of the West Helike Fault segment. Sixteen samples were collected from this sampling site along a 250 m profile starting from the main fault strand at the crest of the fault scarp and across the topset member of the fan-delta deposits (Fig. 3). In this profile we mapped two faults exposing well-defined cores filled with fine-grained sediments. Nine samples were collected from these two fault cores while the remaining samples were from the unaffected protolith. Based on stratigraphic and geomorphological data the displacement hosted by the first order fault is more than 300 m, while the displacement of the second order fault is less than 3 m (Fig. 2). The widths of the fault cores are 0.5 and 0.1 m respectively. Thus the width and displacement in the two fault cores show positive correlation, as has been also observed by several authors (e.g. Shipton and Cowie, 2001).

The XRD patterns of samples collected from the unaffected protolith and the fault cores revealed that the dominant minerals in the fan-delta deposits are calcite and quartz with minor amount of hematite and smectite (Figs. 3D,E). SEM microphotographs show that the grain size of these minerals is typically less than 1 mm.

The samples collected from the two fault cores, six from the main and three from the second order fault core respectively, are reddish to greenish gray in color (Figs. 3B,C). The fault cores are structurally complex and lithologically heterogeneous, comprising a lenses serie of varying color and composition. The boundaries of the lenses are sharp and form acute angles with the fault. More than eight lenses, up to 1-m length and 0.1 m thick were mapped in the core of the first order fault and three in the second order fault cores (Figs. 3B,C). The XRD patterns from the fault core samples revealed higher smectite enrichment in lenses occupying the margins of the faults compared with those found in their central parts (Figs. 3D–F). Macroscopically the smectite rich zones are recognized as greenish gray lenses (Figs. 3C,E). Significant differences were also recognized in the grain size of calcite between samples collected from the margins and the central parts of the fault cores (Figs. 3G1,G2). The calcite grains at the margins of the fault cores measured on SEM microphotographs, was found to be ≈ 1 μm and their grain size increases significantly towards the central parts of the fault core (Figs. 3G1,G2). The reddish color of the material in the two fault cores is due to the presence of Fe-oxides. The abundance of Fe-oxides is very low, as shown by the absence of iron oxide peaks in the XRD data, so that their presence was confirmed only by SEM-EDS. Based on these results; we infer no change in the concentration of iron oxides inside a fault core and the surrounding fan-delta deposits.

In summary, at the Foniskaria sampling site the two fault cores are characterized by high concentration of smectite at their margins that is reduced towards their central parts (Figs. 3G1–G5). In contrast the grain size of calcite increases toward the central part of the fault core. No illite and mixed-layers of illite–smectite were detected. Based on the presence of high amount of smectite at the

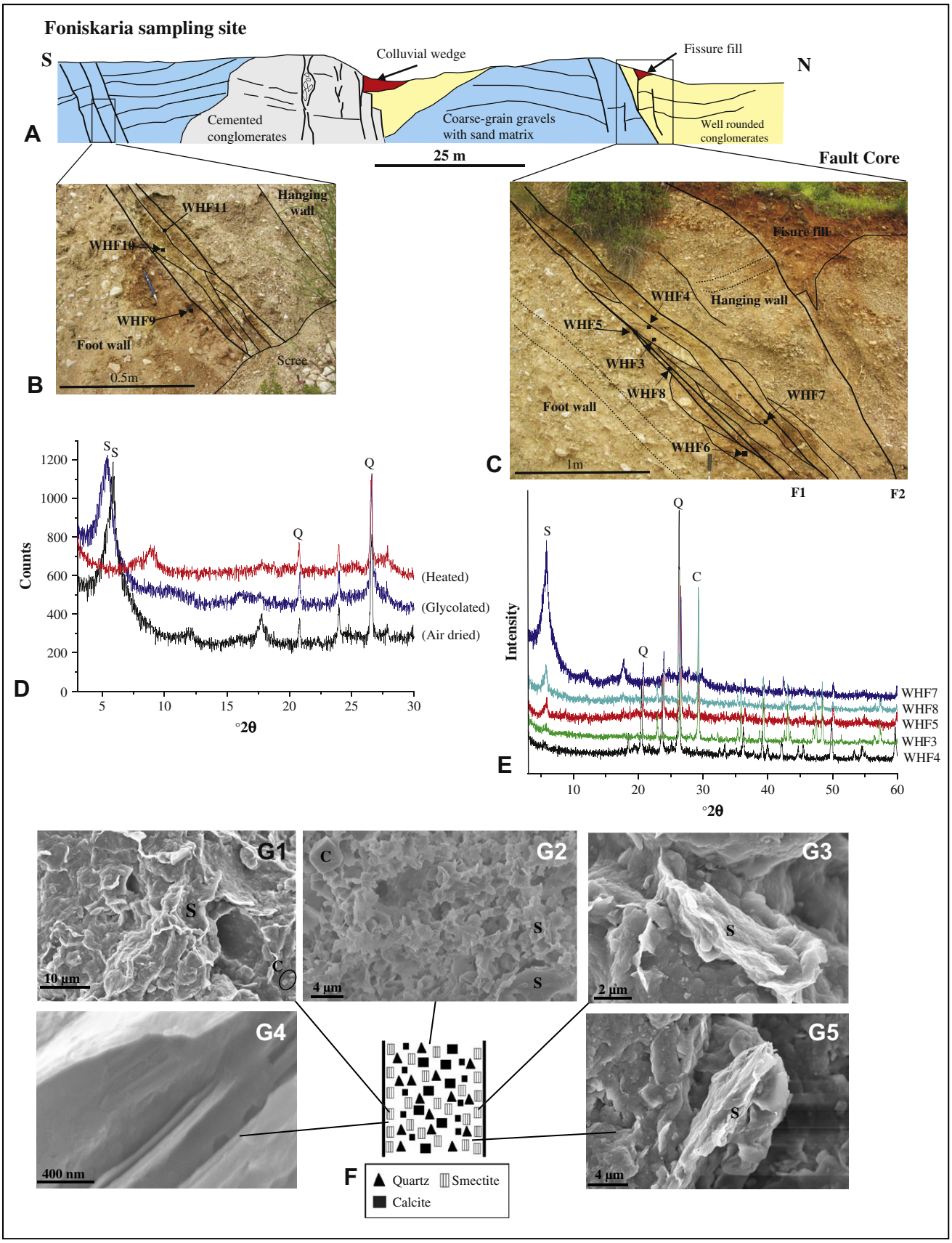

Fig. 3. (A) Cross-section showing first and second order faults at Foniskaria sampling site, for the location of the site see Fig. 2. (B, C) Photos of the second and the first order faults within the Helike Fault zone, showing also locations of samples within the fault cores. Both of the fault cores consist of lenses having remarkable differences in their mineralogical composition. Lenses are aligned at an acute angle to the fault plane. For the location of photos see cross-section (A). (D) XRD patterns of bulk samples showing the dominance of smectite (S) and the presence of quartz (Q) in the fan-delta deposits of the Helike Fault footwall block. (E) XRD patterns of clay fractions showing the differences in their mineralogical composition from the central parts to the margins of the first order fault core. (F) Schematic representation of the distribution of minerals within the fault cores (not to scale). (G1–G5) SEM images of smectite rich samples from the fault cores (S = Smectite, C = micro-calcite). For location of each image see diagram (F). (G1–G2) Smectite flakes and microcalcite, (G3 and G5) smectite showing characteristic flaky shape. (G4) High magnification of a smectite flake.

margins of the fault core, it is inferred that the rims of the fault margins are cemented and sealed to fluid flow.

5.2. The mineralogy near the base of the fault scarp

The mineralogy of samples from the base of the fault scarp was analysed at three locations called hereafter as Nikolaiika, Selinous and T13 (Fig. 2). At the Nikolaiika sampling site, from an 80-m-long artificial cross-section inside a gorge, we sampled three fault cores, as well as the unaffected protolith (Fig. 4). Two of the fault cores belong to second order faults and one to the first order fault (Figs. 4A,B). The first order fault controls a compound fault scarp, as well as a thick colluvial wedge suggesting that this part of the fault was ruptured repeatedly over the recent past (Fig. 4A). The estimated displacement, based on stratigraphic, unpublished geophysical and morphotectonic data is at least 300 m. On the second order faults displacement is on the order of 1 m (Fig. 4B).

From the Nikolaiika sampling site we collected 12 samples from the three fault cores, and 5 from the unaffected protolith (Fig. 4B). The color of all samples is reddish to yellowish. Most of the samples were friable but we were able to collect samples representing the entire width of the 2 second order fault cores. These two samples were epoxy-resin impregnated and analyzed as oriented samples providing thus significant information on the internal structure of the fault core, of the second order faults (Fig. 5). Unfortunately, the sample for the core of the first order fault were friable, probably due to high shearing within the fault and we were not able to obtain oriented samples from this fault core.

XRD patterns of samples from the unaffected protolith revealed the presence of smectite and illite coexisting with calcite, quartz and traces of plagioclases (Fig. 4C). In some samples smectite is present in significant amounts.

Based on XRD patterns (Fig. 4D) and SEM-EDS analyses, the fault core samples are characterized by the presence of plagioclase, quartz, medium-grained calcite and microcrystalline calcite and illite (Figs. 4E,F1–F4). No mixed-layers of illite–smectite were detected. All of the fault zone samples contain Fe-oxides in amounts not detectable by powder XRD, but verified only by SEM microphotographs and SEM-EDS analyses (Fig. 4G). Plagioclase is Na-rich albite, oligoclase. Plagioclase and quartz are primarily concentrated in the central part of the fault core (Figs. 4E,F2). Based on observations of 24 SEM microphotographs, the grain size of quartz is ~0.1 mm at the central part of the fault core and decreases to ~30 μm at its margins (Figs. 4F1,F4). This grain size distribution implies that higher porosity concentrates at the central part of the fault core. In addition their presence in the fault core is rather detrital. SEM observations revealed also the presence of illite flakes in small and stable amount throughout the fault core (Fig. 4F3). The use of the NEWMOD semi-quantitative analysis software suggests that the samples from the margins of the fault core at this sampling site contain a small amount of illite (7%) (the only clay mineral present) and large amounts of micro-calcite (48%) and quartz (45%) (Table 1).

The epoxy-impregnated oriented samples contain a series of lenses ranging in length from a few millimeters to ~4 cm and an aspect ratio of 3.5:1. The lenses are oriented at acute angles to a series of shear zones, spacing apart 1.5 cm (Fig. 5A). The shear planes (dotted lines in the photo of the specimen in Fig. 5) define highly deformed zones composed of a gouge characterized by high calcite precipitation (Fig. 5B). Detailed SEM observations indicate that the amount of calcite present within the lenses outside the gouge is significantly lower (Fig. 5C). Four SEM microphotographs, acquired from the shear zone and the lenses outside it, highlight significant grain size reduction in the shear zone (Fig. 5 microphotographs 1–4). SEM-EDS analyses revealed that plagioclase grains from the gouge and lenses are characterized by different composition. Plagioclases in the gouge is Na-rich (albite and oligoclase) while in the lenses it is andesine. It is out of the purposes of this paper to discuss how these two different types of plagioclases are related with the fluid flow circulation in the fault core. However, the existence or absence of plagioclases in the study area appears to depend on either in the sedimentary succession and the sand fraction in river sediments reflecting possibly its variation in the sediment source (see also Panagos et al., 1978; Katsanou, 2007 unpublished thesis).

At the Selinous River gorge sampling site, located at an elevation of 70 m asl, we collected three samples from the fault core and nine samples from the footwall damage zone (Fig. 6). The mineralogical composition of the flysch in this area does not varies significantly as is indicated from the study of all flysch samples collected from the footwall block. The dominant mineral phases in flysch are calcite, quartz, smectite and illite with no existence of mixed-layers of illite–smectite (Fig. 7). High amount smectite in flysch is common in the Pindos unit elsewhere in Greece (Kisch, 1981).

In the Selinous sampling site the color of the material within both the fault core and the surrounding rocks is greenish gray or reddish (Fig. 6B). The internal structure of the fault core is characterized by the presence of lenses, having their long axes at an acute angle to the fault planes. Their reddish color is due to the presence of small amounts of iron oxides. The absence of iron oxides reflections from the XRD patterns and their identification only by SEM-EDS confirms the above suggestion. The greenish color of the material is attributed to the presence of smectite. XRD and SEM-EDS data from samples collected from the fault core confirm the existence of calcite, quartz, smectite, illite, kaolinite and erionite (Figs. 6C,D1–D4). No mixed-layers of illite–smectite were detected. The minerals within the center of the fault zone constitute of lenses and are oriented sub-parallel to the fault zone. Variations in the amounts of the zeolite group mineral erionite and of the clay minerals smectite, illite and kaolinite from the central part to the margins of the fault core was not detected. The presence of erionite is indicated by XRD data and confirmed by SEM microphotographs and SEM-EDS analyses. Fig. 6D2 presents SEM microphotographs showing the presence of small (≈2 μm) elongate erionite crystal. SEM micrographs and SEM-EDS analyses confirm also the presence of traces of newly formed cerussite ($PbCO_3$) (Fig. 6D1).

It is estimated that, the fault core samples from the Selinous River gorge sampling site, contain about 24% smectite, 12% illite, 11% erionite, 9% kaolinite, 19% calcite and 25% quartz (Table 1). Based on the abundance of the clay minerals in the fault core samples, it is reasonable to assume that the fault is cemented and sealed to the fluid flow.

The T13 sampling site is located at an elevation of 40 m asl, where the Helike Fault juxtaposes fan-delta deposits. It is worth noting that this sampling site is located within a paleoseismological trench excavated across the first order strand of the East Helike Fault segment (Fig. 8). Within this trench, a structureless zone filled with clay rich material was recognized. From this site we collected three samples from the unaffected protolith and three from the first order fault core. The color of the samples from the 10-cm-wide fault core is grayish to reddish.

XRD patterns from the surrounding rocks revealed the coexistence of smectite and traces of illite (Fig. 8C). The mineralogical composition of the fan-delta deposits also includes calcite and quartz with minor amounts of hematite detected only by SEM-EDS. Within the central part of the fault core illite, quartz and medium grained calcite coexist (Figs. 8B,D1,D2). No mixed-layers of illite–smectite were detected. The amount of illite (15%) is significantly higher compared to the unaffected protolith; it is also higher to that

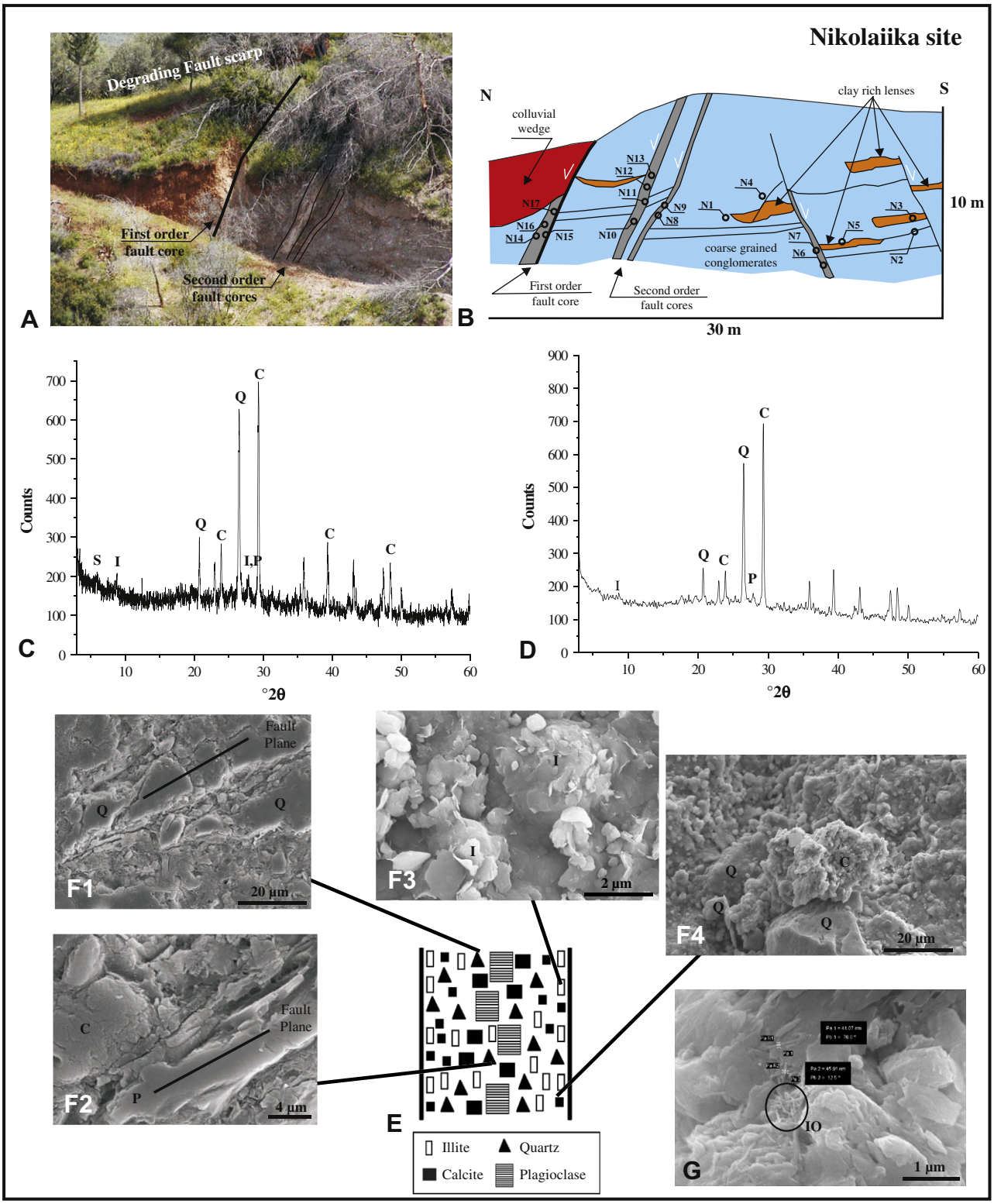

Fig. 4. (A) Outcrop photo of the Nikolaiika sampling site. (B) Cross-section showing a first order and two second order faults at Nikolaiika sampling site, the northern part of the section corresponds to the outcrop photo. (C) XRD pattern of bulk samples showing the presence of quartz (Q), calcite (C), smectite (S), illite (I), and traces of plagioclase, in the unaffected protolith. (D) XRD pattern of bulk samples, showing the presence of calcite (C), quartz (Q), plagioclase (P) and traces of illite (I), in the fault core. (E) Schematic representation of the distribution of minerals within the fault core (not to scale). (F1–F4) SEM images of fault core samples showing parallel alignment along the fault plane of quartz crystals (Q) in image (F1) and of plagioclase crystals (P) in image (F2). Images (F3) show the presence of illite (I), (F4) quartz (Q) and micro-calcite (C). For location of images F1–F4 see diagram (E). (G) SEM image of a fracture surface of a sample from the margin of the fault core, showing the presence of traces of iron oxides (IO).

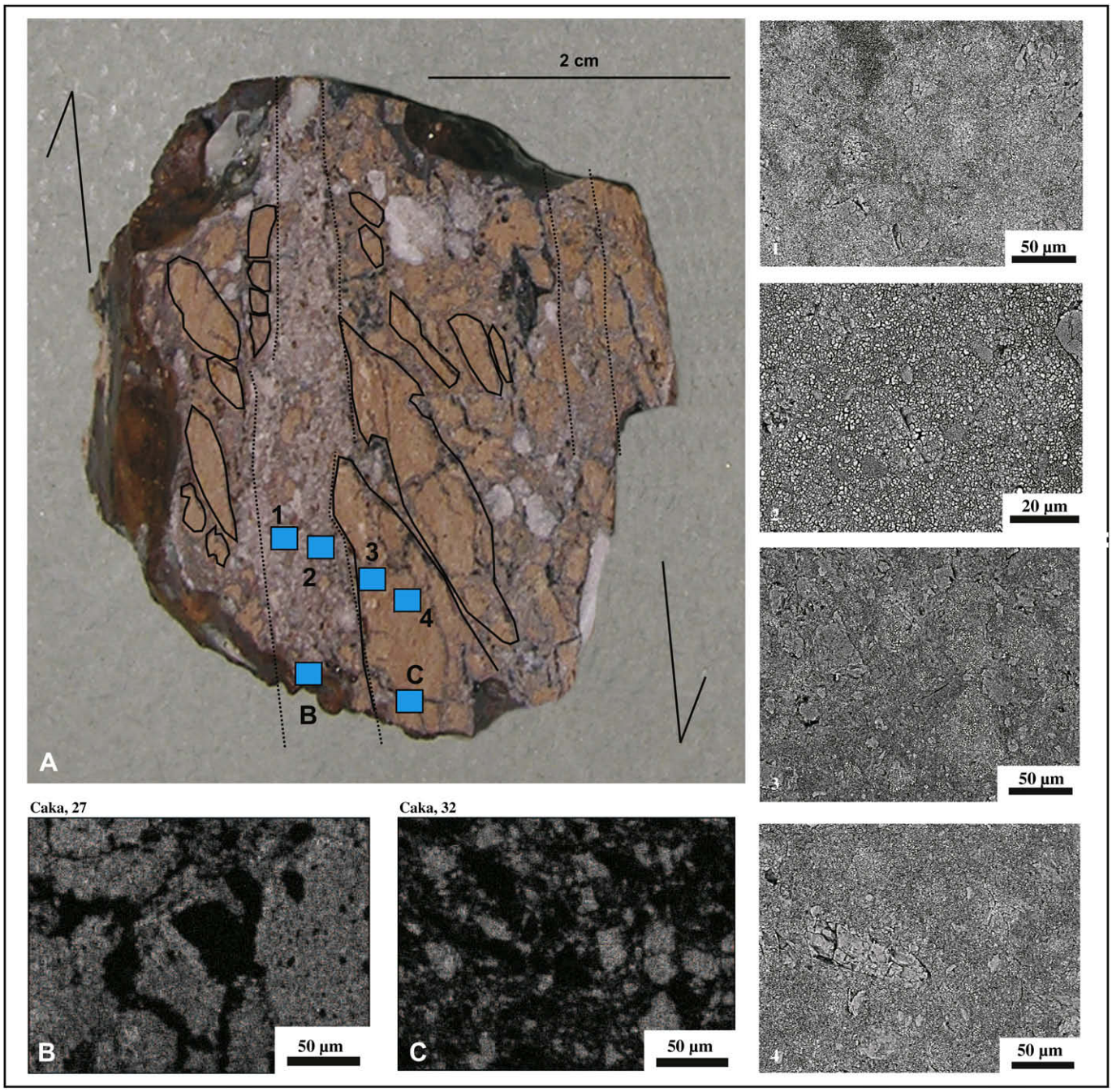

Fig. 5. (A) Polished oriented sample from a fault core treated with epoxy resins. The sample shows gouge zones and a series of lenses. (B, C) Show EDS mapping for the presence of calcite using Ca signals in the fault gouge and the lens at the rims of the zone, respectively. (1–4) Representative SEM images showing grain size in the gouge and in the lenses.

of the Nikolaiika site samples and similar to that of the Selinous River gorge samples (Table 1). As this fault core was built contemporaneously with the accumulation of successive colluvial wedges we suggest that the core was enriched in illite and depleted in smectite in a time interval of about 10 Ka (for details of dating see Koukouvelas et al., 2005).

In summary, the amount of clay minerals at the base of the fault scarp is relatively low (7 and 15% correspondingly) compared to their amount at the crest of the footwall block (83%) (Table 1). The absence of erionite, kaolinite and plagioclase from the T13 sampling site is a striking difference between the T13 and the Selinous gorge sampling sites, although, both of them are approximately at the

Table 1
Quantitative analyses of samples collected in the fault core in all sampling sites using NEWMOD ©.

Position	Mineralogical composition (%), calculated using NEWMOD					
	Smectite	Illite	Kaolinite	Erionite	Quartz	Calcite
Foniskaria	83	–	–	–	17	–
Nikolaiika	–	7	–	–	45	48
Selinous	24	12	9	11	25	19
T13	–	15	–	–	39	46

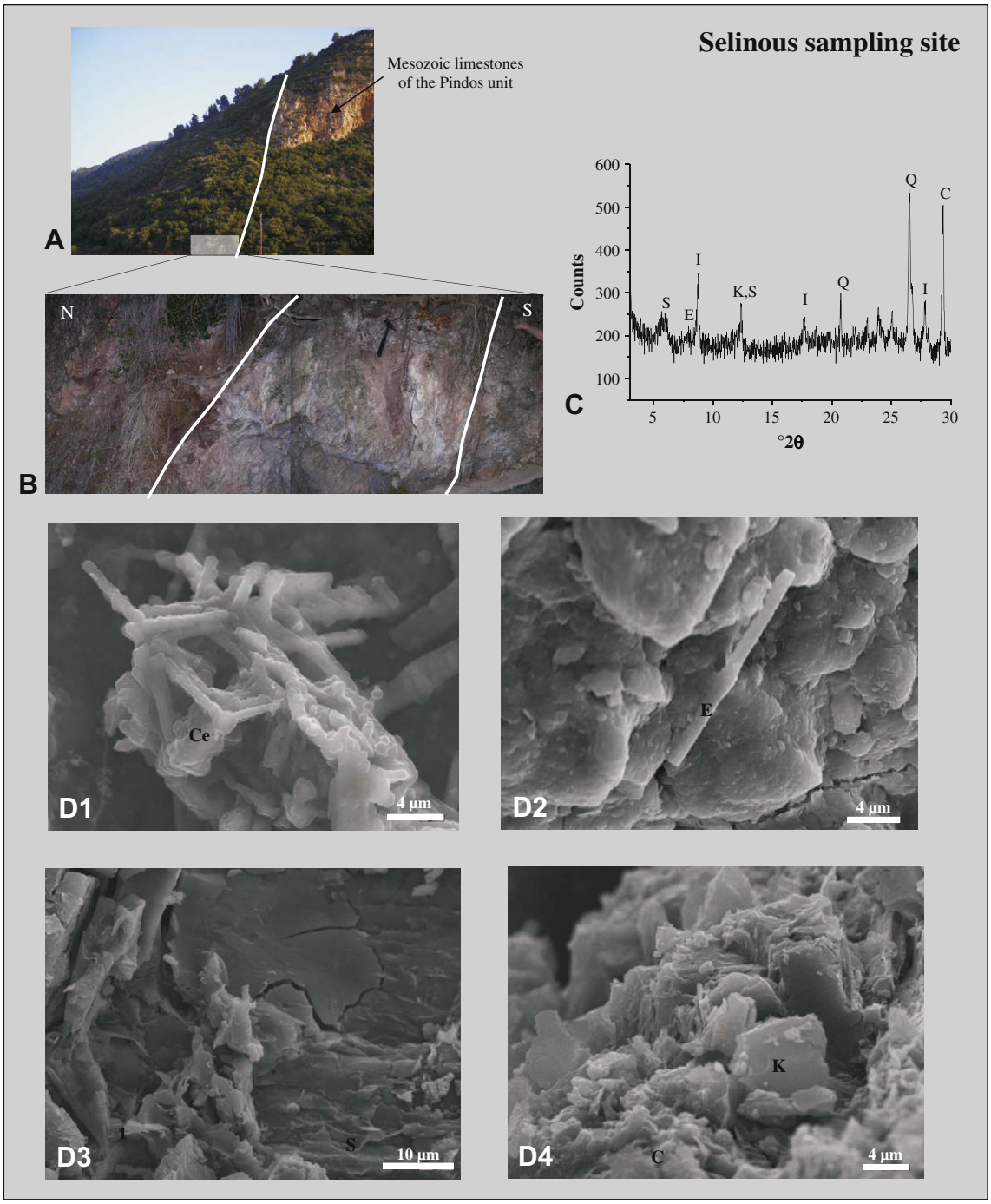

Fig. 6. (A) Outcrop photo of Selinous sampling site. (B) Detail of the Helike Fault core at Selinous sampling site. (C) XRD pattern of a bulk sample showing the presence of smectite (S), illite (I), erionite (E), kaolinite (K), quartz (Q) and calcite (C). (D1–D4) SEM images of a cerussite (Ce) crystal (D1), a tubular erionite (E) (D2), (D3) shows the coexistence of smectite (S) and illite (I) flakes and (D4) shows a book-type kaolinite (K) and grains of micro-calcite (C).

same elevation, or at a similar structural depth. This could be attributed to differences in fluid flow circulation through the two fault segments. However, giving that our data comprise only one site on the East Helike Fault segment is not robust to infer or to exclude differences between the mineralogical compositions of the two fault segments.

6. Discussion

The westernmost end of the Gulf of Corinth is a key area for understanding physics of earthquakes in extensional settings because this area is characterized by high seismicity, and spectacular fault outcrops. The current study offers new data for the role of the clay mineralogy during the earthquake cycle along the Helike Fault. In addition, we use published data for clay minerals within the fault cores of the Aigion and Pyrgaki Faults to draw conclusions for all three faults that constitute a fault array accommodating significant part of the current extension within the western part of the Gulf of Corinth (Koukouvelas et al., 2001; Micarelli et al., 2003; McNeill et al., 2007). Our work is based on near-surface sampling in a setting that is affected by undergoing exhumation and thus any result has to be treated carefully because it is possible that the

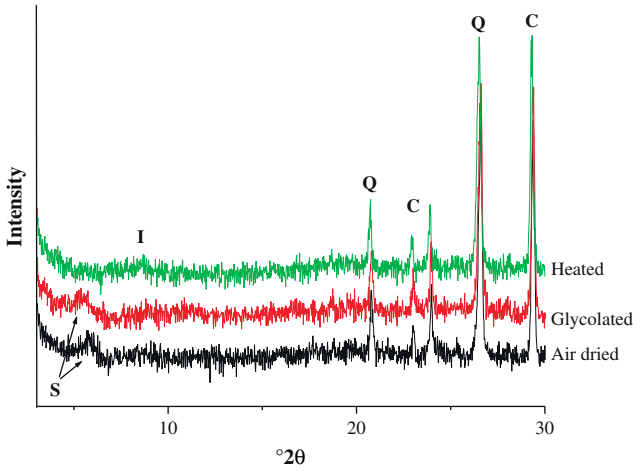

Fig. 7. Three XRD patterns of the clay fractions in the Pindos unit flysch, showing the presence of quartz (Q), calcite (C) and smectite (S). After thermal treatment of the sample smectite transforms to illite (I).

material sampled may not be adequately represent due to weathering, the materials at depth (see also discussion in Sibson, 2000).

6.1. Fluid flow and mineralogy of the fault damage zone

The mineralogy of the fault core reveals the presence of a series of the following minerals smectite, illite, quartz, calcite, plagioclase, kaolinite, cerussite and erionite and the absence of mixed-layer illite–smectite. Smectite, a common mineral in shallow sediments, is concentrated at the crest of the footwall, while the presence of illite is relatively more abundant at the lower part of the fault scarp. The source of these minerals is probably the Pindos Unit flysch and the Pliocene fan-delta deposits as is revealed from the XRD data in 15 samples collected from the footwall block and published data from flysch deposits in central Greece (Kisch, 1981). The coexistence of plagioclase, smectite and erionite indicate intermediate to alkaline type of alteration, at low cation/hydrogen ratios in the solution, suggesting that the formation of kaolinite in these conditions is not possible (Utada, 1980; Inoue, 1995). Therefore, it is concluded that kaolinite is also of detrital origin. The cerussite probably highlight meteoric water circulation. From this point and onwards we will define smectite, illite, quartz, plagioclases, calcite and kaolinite as "pre-existing" minerals highlighting preferable meteoric and/or phreatic water circulation through the rims of the fault core. In contrast erionite is recognized only in the fault cores, as a newly formed mineral due to hydrothermal activity. In addition, as most of the minerals are significantly increased in the fault cores we suggest that the fault core is acting more or less as a significant path for downward moving fluids (Fig. 9). In accordance with the mineralogy composition is a series of hydrogeological experiments in the area around the Helike Fault. These hydrogeological experiments in the area suggest strong meteoric signature with their geochemical composition of the water including low Eh values, high CO_2 and water slight enrichment in H_2S, SO_4, NH_4 and B contents (Giurgea et al., 2004; Pizzino et al., 2004). B contents according to Pizzino et al. (2004) indicate the

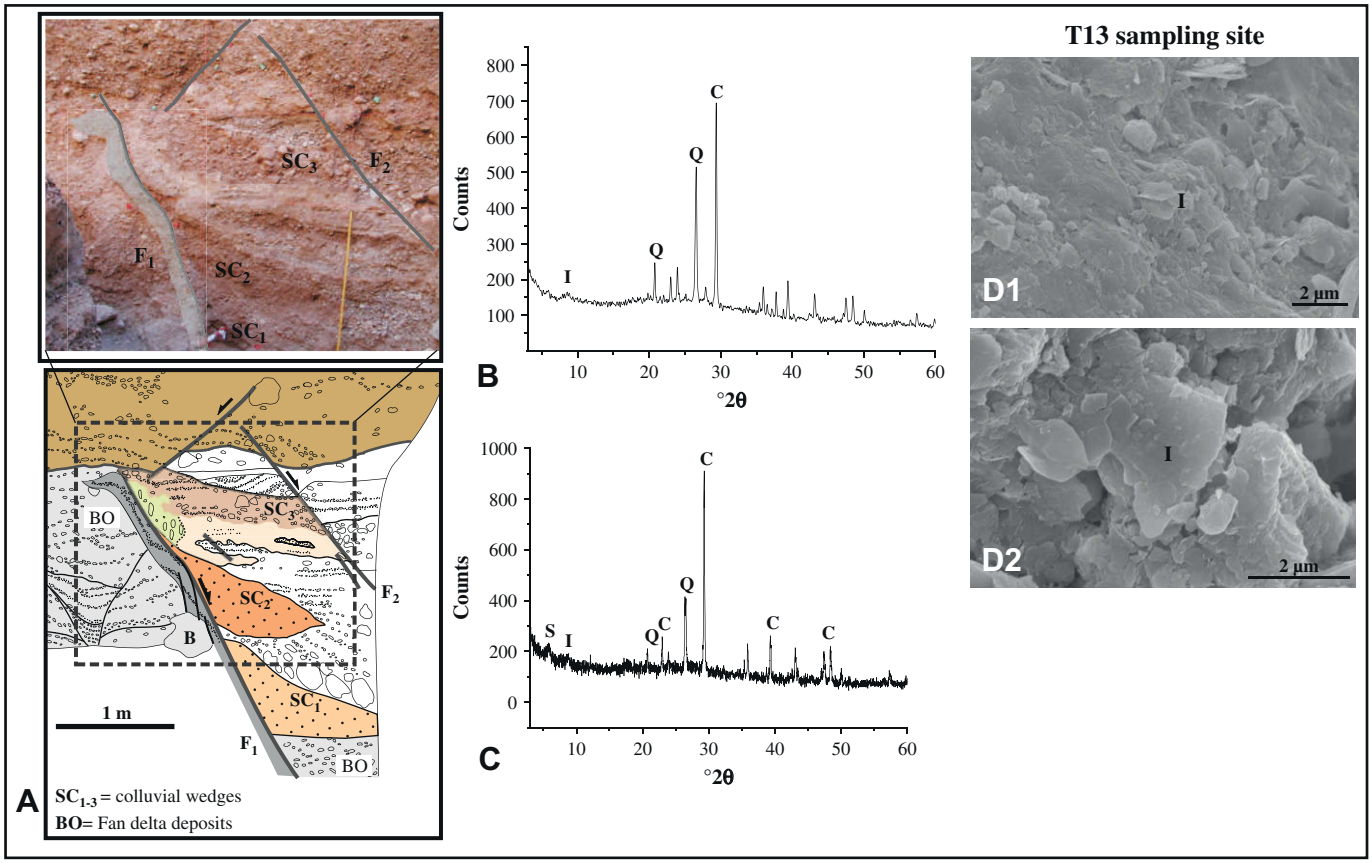

Fig. 8. (A) Outcrop photo of T13 sampling site (adapted from Koukouvelas et al., 2005). (B) XRD pattern of a bulk sample showing the presence of illite (I), quartz (Q) and calcite (C) in the fault zone. (C) XRD pattern of a bulk sample showing the presence of smectite (S), illite (I), calcite (C) and quartz (Q) in the unaffected protolith. (D1–D2) SEM images showing the presence of illite (I) flakes within the fault core.

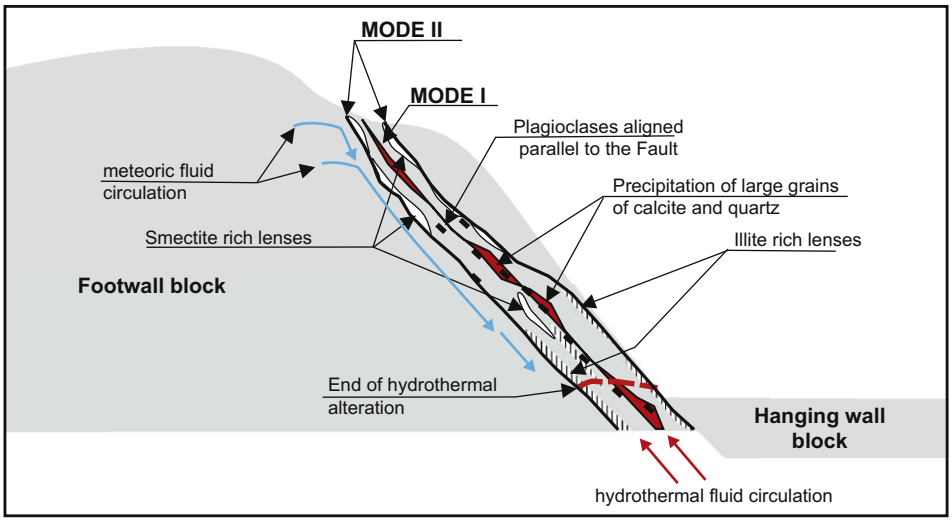

Fig. 9. Diagramatic model showing mineral distribution and fluid flow circulation in the Helike Fault zone.

upward movement of deeply originated fluids through a permeable pathway called also a "geochemically active fault zone". The geochemistry of waters in combination with mineralogy is considered as an unequivocal proof for downward and upward moving fluids through the fault.

Regarding the grain size analysis within the fault, mineral particles at all sampling sites appear to increase in size from the rims to the center of the fault core. This suggests precipitation of new material in the center of the fault core in Mode I cracks. Smectite or illite parallelization with the fault plane suggests shearing in the rims of fault cores (Fig. 9). These two lines of evidences suggest precipitation of new material in the center of the fault core along with continuing shear at its rims.

The concentration of smectite within the rims of the fault core in its upper part suggests that clay minerals are significant to the formation of permeability barrier along the fault. A remarkable result of our analysis is that illite progressively increases downwards along with a smectite decrease. This smectite decrease or illite increase with depth can be probably attributed to the meteoric water circulation through the fault.

According to published data the mineralogy of the Pyrgaki Fault core samples is characterized by the presence of illite, kaolinite, chlorite and zeolites while in the unaffected protolith mixed-layer illite–smectite, kaolinite and chlorite are common (Géraud et al., 2006). The Aigion Fault core samples are characterized by the presence of illite, chlorite and albite (Sulem et al., 2005). Thus, the mineralogy of all faults appears to be similar, with the exception of that of Helike Fault core which shows a remarkable absence of chlorite and mixed-layer illite–smectite.

6.2. Intensity of hydrothermal alteration

The exposed crustal section of the Helike Fault is characterized by the existence of a series of detrital and newly formed minerals that provide information on the temperature and chemistry of fluids flowing through the fault. Particularly important for the definition of the fault's core temperature is the absence of mixed-layer illite–smectite and the existence of erionite. The absence of mixed-layer illite–smectite within the fault core indicates that the temperature never reached or exceeded 100 °C. This is because if the temperature was higher than 100 °C at least partially, smectite would have been converted to mixed-layer illite–smectite and in even higher temperatures to illite either due to hydrothermal activity or shear heating (Srodon and Eberl, 1984; Hashimoto et al., 2007). Erionite is a zeolite characteristic of hydrothermal alteration and its presence indicates that the temperature range was between 80 and 120 °C (Osinski, 2005). The absence of mixed-layer illite–smectite and the existence of erionite indicate fluid temperatures in the interval of 80–100 °C.

In the deeper parts of the Helike Fault, calcite, quartz, cerussite, smectite, kaolinite, illite and erionite coexist. The presence of kaolinite, combined with the absence of dickite (kaolinite polymorph formed at higher temperatures) in the fault core similarly suggests that temperature has never exceeded 100 °C. Kaolinite transforms to dickite as temperature increases in fault zones as it is common elsewhere in Greece (e.g. Papoulis and Tsolis-Katagas, 2001; Papoulis et al., 2004, 2005). Erionite is usually the alteration product of volcanic glass or feldspars or poorly crystalline clay minerals (Dogan, 2003). The erionite is sensitive to the alkalinity of the system and is stable only at a limited range of thermochemical conditions (Birsoy, 2002). However, the absence of volcanic rocks in obvious proximity to the study area and of poorly crystalline clay minerals in the fault core indicates that probably the induced mineral alteration was commenced at deeper levels in the crust.

In addition the rare existence of erionite suggests that this temperature within the fault core is local due to infiltration of hydrous fluids within the fault core. This high temperature outlasted for short, probably corresponding to the phase (δ) and induced mineral alternation and reaction weakening in the fault zone during the phase (α) of the seismic cycle, respectively. Furthermore, the presence of erionite only at the Selinous River gorge sampling site and its absence at the structurally similar T13 sampling site, probably indicate significant changes in the hydrothermal alteration and the fluid flow between the two segments of the fault.

6.3. Fluid circulation and seismicity within the westernmost end of the Gulf of Corinth

Our data intergraded with the crust structure appears to shed light on how the faults interact with fluids in this area (Fig. 9). In detail, seismic tomography data, magneto-telluric modeling and geological studies in the area suggest that phyllites are located at a depth greater than 5-km under the Gulf (Latorre et al., 2004). The Moho depth in the study area is about 37.5 km (Sachpazi et al.,

2007, their Fig. 5). Based on modeling, the temperature of the upper part of the Moho is 560 °C (Westaway, 2007). Temperature data at depth, derived from the AIG10 well suggest a temperature of 32 °C at a depth of 750 m on the Aigion Fault (Doan and Cornet, 2007). Based on these data the probable geothermal gradient in the area is 15 °C/km. Assuming such a value for the geothermal gradient we infer that occasionally the fluid circulation probably affects a significant part of the crust.

The historic seismicity of the area indicates that the Helike and Aigion Faults are hosting strong and moderate earthquakes, respectively (Koukouvelas and Doutsos, 1996; Bernard et al., 1997; Koukouvelas et al., 2005). The Pyrgaki Fault host rather limited seismicity and moderate earthquakes (Zahradník et al., 2004; Pacchiani and Lyon-Caen, 2007). However, since all faults control fan-deltas, with the Helike and Aigion Faults characterized by high slip rate, it is reasonable to suggest that the Pyrgaki Fault was much more seismically active in the past (Roberts and Koukouvelas, 1996; Pantosti et al., 2004; Koukouvelas et al., 2005). If we assume the zeolites in the Helike (70 m asl) and the Pyrgaki Faults (700 m asl), respectively, as homologous points in terms of their depth of formation and temperature, then the Pyrgaki Fault is older and more exhumed than the Helike Fault. Accepting an uplift rate in the order of 1 mm/yr, then the age of the Pyrgaki is ~0.65 Ma older than the Helike Fault. In addition, the presence of mixed-layer illite–smectite in the unaffected protolith away the Pyrgaki Fault probably suggests that shear heating is not recognized in the exposed part of the Pyrgaki and Helike Faults.

The existence of the zeolites in the fault cores suggests upward moving fluids from depth, probably through the fault core during repeated earthquakes. However, the comparison of the mineralogical composition between the Pyrgaki and Aigion Faults and the presence of significant quantities of chlorite along their cores suggest deeper fluid circulation in these faults.

6.4. A candidate model

Among the acceptable models for the explanation of the mineralogy within the fault cores, we consider the "fault-valve model" as the most appropriate. For the "fault-valve model" to be applicable the existence of permeability barriers in the upper crust is appropriate (e.g. Sibson, 1990). Observations in the AIG10 deep borehole that crosses the Aigion Fault and hydrogeological data for the Helike Fault suggest permeability differences between the fault core, the damage zone of faults and the surrounding rocks (Giurgea et al., 2004; Micarelli et al., 2006; Doan and Cornet, 2007). According to the "fault-valve model" a high postfailure permeability is expected, hydrothermal precipitation along the discharge path that is the fault core or closely spaced fault strands (Sibson, 2007). In this model the maintenance of permeability barrier is re-established by precipitation of clay minerals within the fault core and the fault sealing (e.g. Warr and Cox, 2001). This fluid circulation is established in the upper 5-km depth of the crust. However, evidence for even deeper circulation within the faults is probably inferred by the existence of chlorite in Aigion and Pyrgaki Faults that we do not confirm for the Helike Fault.

Several lines of evidence supporting the involvement of overpressured fluids in the study area include: (1) the swarm-like character of the earthquake sequence of the 2001 seismicity crisis in the area between Pyrgaki and Helike Faults (Lyon-Caen et al., 2004); (2) the reactivation of NW-trending and thus unfavorably oriented faults in this 2001-seismic crisis which is characterized by the migration of seismic activity towards the surface (Pacchiani and Lyon-Caen, 2007); and (3) geophysical anomalies consistent with distributed overpressuring in the lower crust close to the end of the seismogenic zone (Latorre et al., 2004).

In summary, there are striking lines of evidence that earthquakes in the study area occur within an overpressured crust but it is also likely that fluid-overpressuring was compartmentalized and quite heterogeneous within the Helike, the Pyrgaki and the Aigion Faults, accommodating the extension in this part of the Gulf of Corinth.

7. Conclusions

Our study offers data for fluid circulation in the upper part of the Helike Fault. The Helike Fault is a crustal scale fault having first and second order faults organized into a fault zone.

(1) The internal structure of the Helike Fault core appears to vary from lenticular to chaotic in an exposed section of 500 m. First order as well as some of the second order faults are characterized by a clay-rich fault core.
(2) The fault is juxtaposing rocks of the Pindos unit at the surface, which are considered to be source rocks for the syn-rift sediments and contain typically smectite, illite, quartz, plagioclases and calcite. The mineralogical composition of samples from the fault cores differ in enrichment of smectite and illite. The smectite rich part is 400 m in height, while the illite rich zone is exposed at more or less 100-m-height. Other minerals recognized only within the fault cores are cerussite, kaolinite and erionite.
(3) Erionite recognized only in the fault cores samples suggests upward fluid flow through the fault cores and weak hydrothermal alteration.
(4) Samples from the core of the Helike Fault contain a relatively low amount of clay minerals that play a crucial role in the slip of the fault during earthquakes. The downward meteoric water infiltration is testified by the precipitation of calcite and cerussite and the upwelling of fluids by the precipitation of erionite. The central parts of the fault host coarser grained minerals suggesting that this is the part of the core with the higher permeability.
(5) The upper part of Helike Fault acts as a channel during earthquake for fluid infiltration. The presence of smectite in the margins of the upper part of the fault confines fluids to the fault core and prevents them from escaping through zones of otherwise fractured host rock.
(6) The Helike Fault is a major fault in the area of the Gulf of Corinth where fluid redistribution by fault-valve action seems likely to have occurred over its evolution.

Acknowledgements

The authors wish to thank Mr. V. Kotsopoulos, of the Laboratory of Electron Microscopy and Microanalysis, University of Patras, for his help with the microanalyses and the SEM micrographs. This contribution is benefited by stimulating discussion and reading of earlier versions by Christos Katagas, Sotiris Kokkalas. We are also grateful to journal reviewer Kyu Kanagawa for valuable suggestions as well as to Editor Jao Hippertt for his assistance.

References

Agosta, F., Prasad, M., Aydin, A., 2007. Physical properties of carbonate fault rocks, fucino basin (Central Italy): implications for fault seal in platform carbonates. Geofluids 7, 19–32.
Aydin, A., 2000. Fractures, faults, and hydrocarbon entrapment, migration and flow. Marine and Petroleum Geology 17, 797–814.
Berg, S.S., Skar, T., 2005. Controls on damage zone asymmetry of a normal fault zone: outcrop analyses of a segment of the Moab fault, SE Utah. Journal of Structural Geology 27, 1803–1822.

Bernard, P., Briole, P., Meyer, B., Lyon-Caen, H., Gomez, J.-M., Tiberi, C., Berge, C., Cattin, R., Hatzfeld, D., Lachet, C., Lebrun, B., Deschamps, A., Courboulex, F., Laroque, C., Rigo, A., Massonnet, D., Papadimitriou, P., Kassaras, J., Diagourtas, D., Makropoulos, K., Veis, G., Papazisi, E., Mitsakaki, C., Karakostas, V., Papadimitriou, P., Papanastassiou, D., Chouliaras, G., Stavrakakis, G., 1997. The Ms = 6.2, June 15, 1995 Aigion earthquake (Greece): evidence for low angle normal faulting in the Corinth rift. Journal of Seismology 1, 131–150.

Bernard, P., Lyon-Caen, H., Briole, P., Deschamps, A., Boudin, F., Makropoulos, K., Papadimitriou, P., Lemeille, F., Patau, G., Billiris, H., Paradissis, D., Papazissi, K., Castarède, H., Charade, O., Nercessian, A., Avallone, A., Pacchiani, F., Zahradnik, J., Sacks, S., Linde, A., 2006. Seismicity, deformation and seismic hazard in the western rift of Corinth: new insights from the Corinth Rift Laboratory (CRL). Tectonophysics 426, 7–30.

Birsoy, R., 2002. Activity diagrams of zeolites: implications for the occurrences of zeolites in Turkey and of Erionite worldwide. Clays and Clay Minerals 50, 136–144.

Briole, P., Rigo, A., Lyon-Caen, H., Ruegg, J.C., Papazissi, K., Mitsakaki, C., Balodimou, A., Veis, G., Hatzfeld, D., Deschamps, A., 2000. Active deformation of the Corinth rift, Greece: results from repeated Global Positioning System surveys between 1990 and 1995. Journal of Geophysical Research 105, 25605–25625.

Burton, P.W., Xu, Y., Qin, C., Tselentis, G.-A., Sokos, E., 2004. A catalogue of seismicity in Greece and the adjacent areas for the twentieth century. Tectonophysics 390, 117–127.

Byerlee, J., 1993. Model for episodic flow of high-pressure water in fault zones before earthquakes. Geology 21, 303–306.

Caine, J.S., Evans, J.P., Forster, C.B., 1996. Fault zone architecture and permeability structure. Geology 11, 1025–1028.

Chester, F.M., Evans, J.P., Biegel, R.L., 1993. Internal structure and weakening mechanisms of the San Andreas fault. Journal of Geophysical Research 98, 771–786.

Davatzes, N.C., Aydin, A., 2005. Distribution and nature of fault architecture in a layered sandstone and shale sequence: an example from the Moab fault, Utah. In: Sorkhabi, R., Tsuji, Y. (Eds.), Faults, Fluid Flow, and Petroleum Traps. American Association of Petroleum Geologists Memoir, 85, pp. 153–180.

Doan, M.L., Cornet, F.H., 2007. Thermal anomaly near the Aigio fault, Gulf of Corinth, Greece, maybe due to convection below the fault. Geophysical Research Letters 34, L06314, doi:10.1029/2006GL028931.

Dogan, A.U., 2003. Zeolite mineralogy and Kappadocian Erionite. Indoor and Built Environment 12, 337–342.

Doutsos, T., Kokkalas, S., 2001. Stress and deformation in the Aegean region. Journal of Structural Geology 23, 455–472.

Doutsos, T., Poulimenos, G., 1992. Geometry and kinematics of active faults and their seismotectonic significance in the western Corinth-Patras rift (Greece). Journal of Structural Geology 14, 689–699.

Doutsos, T., Koukouvelas, I., Poulimenos, G., Kokkalas, S., Xypolias, P., Skourlis, K., 2000. An exhumation model of the south Peloponnesus, Greece. International Journal of Earth Science 89, 350–365.

Doutsos, T., Koukouvelas, I.K., Xypolias, P., 2006. A new orogenic model for the External Hellenides. In: Robertson, A.H.F., Mountrakis, D. (Eds.), Tectonic Development of the Eastern Mediterranean Region. Geological Society, Special Publications, vol. 260, pp. 507–520.

Fitts, T.G., Brown, K.M., 1999. Stress-induced smectite dehydration: ramifications for patterns of freshening and fluid expulsion in the N. Barbados accretionary wedge. Earth and Planetary Science Letters 172, 179–197.

Gallousi, C., Koukouvelas, I.K., 2007. Quantifying geomorphic evolution of earthquake-triggered landslides and their relation to active normal faults. An example from the Gulf of Corinth, Greece. Tectonophysics 440, 85–104.

Gautschi, A., 2000. Hydrogeology of a fractured shale (Opalinus clay): implications for deep geological disposal of radioactive wastes. Hydrogeology Journal 9, 97–107.

Géraud, Y., Diraison, M., Orellana, N., 2006. Fault zone geometry of a mature active normal fault: a potential high permeability channel (Pirgaki fault, Corinth Rift, Greece). Tectonophysics 426, 31–59.

Giurgea, V., Rettenmaier, D., Pizzino, L., Unkel, I., Hötzl, H., Förster, A., Quattrocchi, F., 2004. Preliminary hydrogeological interpretation of the Aigion area from the AIG10 borehole data. Comptes Rendus Geosciences 336, 467–475.

Hashimoto, Y., Ujiie, K., Sakaguchi, A., Tanaka, H., 2007. Characteristics and implication of clay minerals in the northern and southern parts of the Chelung-pu fault, Taiwan. Tectonophysics 443, 233–242.

Hatzfeld, D., Karakostas, V., Ziazia, M., Kassaras, I., Papadimitriou, E., Makropoulos, K., Voulgaris, N., Papaioannou, C., 2000. Microseismicity and faulting geometry in the Gulf of Corinth (Greece). Geophysical Journal International 141, 438–456.

Hickman, S., Sibson, R., Bruhn, R., 1995. Introduction to special section: mechanical involvement of fluids in faulting. Journal of Geophysical Research 100, 12831–12840.

Holness, M.B., 1997. Deformation-enhanced Fluid Transport in the Earth's Crust and Mantle. In: Mineralogical Society Series, 8. Chapman & Hall, London.

Hubbert, M.K., Rubey, W.W., 1959. Role of fluid pressure in mechanics of over thrust faulting. Geological Society of America Bulletin 70, 115–166.

Inoue, A., 1995. Formation of clay minerals in hydrothermal environments. In: Velde, B. (Ed.), Clays and the Environment: Origin and Mineralogy of Clays. Springer, pp. 268–329.

Jourde, H., Cornaton, F., Pistre, S., Bidaux, P., 2002. Flow behavior in a dual fracture network. Journal of Hydrology 266, 99–119.

Kahr, G., Kraehenbuehl, F., Stoeckli, H.F., Muller-Vonmoos, M., 1990. Study of the water-bentonite system by vapour adsorption, immersion calorimetry and X-ray techniques: II. Heats of immersion, swelling pressures and thermodynamic properties. Clay Minerals 25, 499–506.

Katsanou, K., 2007. Environmental hydrogeological conditions of the drainage basins in the Aigion area using hydrochemical methods. Unpublished M.Sc. thesis, University of Patras.

Kisch, H., 1981. Burial diagenesis in tertiary "flysch" of the external zones of the Hellenides in central Greece and the Olympos region, and its tectonic significance. Eclogae Geologicae Helvetiae 74, 603–624.

Koch, U., Heinicke, J., Vossberg, M., 2003. Hydrogeological effects of the latest Vogtland-NW Bohemian swarmquake period (August to December 2000. Journal of Geodynamics 35, 107–123.

Kokkalas, S., Xypolias, P., Koukouvelas, I.K., Doutsos, T., 2006. Post-collisional contractional and extensional deformation in the Aegean region. In: Dilek, Y., Pavlides, S. (Eds.), Post-Collisional Tectonics and Magmatism in the Mediterranean region and Asia. Geological Society of America Special Paper, vol. 409, pp. 97–123.

Koukouvelas, I.K., 1998. The Egion fault, earthquake-related and long-term deformation, Gulf of Corinth, Greece. Journal of Geodynamics 26, 501–513.

Koukouvelas, I.K., Doutsos, T., 1996. Implication of structural segmentation during earthquakes: the 1995 Egion earthquake, Gulf of Corinth, Greece. Journal of Structural Geology 18, 1381–1388.

Koukouvelas, I.K., Roberts, G., 2007. Preface: deep structure, fault arrays and surface processes within an active graben: The Gulf of Corinth. Tectonophysics 440, 1–4.

Koukouvelas, I.K., Stamatopoulos, L., Katsonopoulou, D., Pavlides, S., 2001. A paleoseismological and geoarchaeological investigation of the Eliki fault, Gulf of Corinth, Greece. Journal of Structural Geology 23, 531–543.

Koukouvelas, I.K., Katsonopoulou, D., Soter, S., Xypolias, P., 2005. Slip rates on the Helike Fault, Gulf of Corinth, Greece: new evidence from geoarchaeology. Terra Nova 17, 158–164, doi:10.1111/j.1365-3121.2005.00603.x.

Latorre, D., Virieux, J., Monfret, T., Monteiller, V., Vanorio, T., Got, J.-L., Lyon-Caen, H., 2004. A new seismic tomography of Aigion area Gulf of Corinth, Greece from a 1991 data set. Geophysical Journal International 159, 1013–1031.

Lyon-Caen, H., Papadimitriou, P., Deschamps, A., Bernard, P., Makropoulos, K., Pacchiani, F., Patau, G., 2004. First results of the CRLN seismic network in the western Corinth Rift: evidence for old-fault reactivation. Comptes Rendus Geosciences 336, 343–351.

Matthäi, S.K., Aydin, A., Pollard, D.D., Roberts, S.G., 1998. Numerical simulation of departures from radial drawdown in a faulted sandstone reservoir with joints and deformation bands. In: Jones, G., Fisher, Q.J., Knipe, R.J. (Eds.), Faulting, Fault Sealing, and Fluid Flow in Hydrocarbon Reservoirs. Geological Society, London, Special Publications, vol. 147, pp. 157–191.

McNeill, L.C., Cotterill, C.J., Bull, J.M., Henstock, T.J., Bell, R., Stefatos, A., 2007. Geometry and slip rate of the Aigion fault, a young normal fault system in the western Gulf of Corinth. Geology 7, 355–358, doi:10.1130/G23281A.1.

Micarelli, L., Moretti, I., Daniel, J.M., 2003. Structural properties of rift-related normal faults: the case study of the Gulf of Corinth, Greece. Journal of Geodynamics 36, 275–303.

Micarelli, L., Moretti, I., Jaubert, M., Moulouel, H., 2006. Fracture analysis in the south-western Corinth rift (Greece) and implications on fault hydraulic behavior. Tectonophysics 426, 31–59.

Miller, S.A., Collettini, C., Chiaraluce, L., Cocco, M., Barchi, M., Kaus, B.J.P., 2004. Aftershocks driven by a high-pressure CO2 source at depth. Nature 427, 724–727.

Moretti, I., Sakellariou, D., Lykousis, V., Micarelli, L., 2003. The Gulf of Corinth: an active half graben? Journal of Geodynamics 36, 323–340.

Noda, H., Shimamoto, T., 2005. Thermal pressurization and slip-weakening distance of a fault: an example of the Hanaore fault, southwest Japan. Bulletin of the Seismological Society of America 95, 1224–1233.

Osinski, G.R., 2005. Hydrothermal activity associated with the Ries impact event, Germany. Geofluids 5, 202–220.

Pacchiani, F., Lyon-Caen, H., 2007. Earthquake migration within a normal fault and implications on rock permeability. Geophysical Research Abstracts, 9, SRef-ID: 1607–7962/gra/EGU2007-A-07841.

Panagos, A.G., Pe, G.G., Gerouki, F., 1978. Detrital mineralogy of river sands, Peloponnese, Greece. Neus Jahrbuch fur Mineralogie Monatshefte 1978, 447–454.

Pantosti, D., DeMartini, P., Koukouvelas, I.K., Stamatopoulos, L., Palyvos, N., Pucci, S., Lemeille, F., Pavlides, S., 2004. Palaeoseismological investigations of the Aigion Fault (Gulf of Corinth, Greece). Comptes Rendus Geoscience 336, 335–342.

Papoulis, D., Tsolis-Katagas, P., 2001. Kaolinization process in the rhyolitic rocks of Kefalos, Kos island, Aegean sea, Greece. Bulletin of Geological Society of Greece 34, 867–874.

Papoulis, D., Tsolis-Katagas, P., Katagas, C., 2004. Monazite alteration mechanisms and depletion measurements in kaolins. Applied Clay Science 24, 271–285.

Papoulis, D., Tsolis-Katagas, P., Tsikouras, B., Katagas, C., 2005. An FT-Raman, Raman and FTIR study in Hydrothermally altered volcanic rocks from Kos island (Southeastern Aegean, Greece). In: Fytikas, M., Vougioukalakis, G. (Eds.), Developments in Volcanology, vol. 7. Elsevier, pp. 293–304.

Pavlides, S., Koukouvelas, I.K., Kokkalas, S., Stamatopoulos, L., Keramydas, D., Tsodoulos, I., 2004. Late Holocene evolution of the East Eliki Fault, Gulf of Corinth (Central Greece). Quaternary International 115-116, 139–154.

Pham, V.N., Bernard, P., Boyer, D., Chouliaras, G., Le Mouël, J.-L., Stavrakakis, G.N., 2000. Electrical conductivity and crustal structure beneath the central

Hellenides around the Gulf of Corinth (Greece) and their relationship with the seismotectonics. Geophysical Journal International 142, 948–969.
Pili, E., Poitrasson, F., Gratier, J.-P., 2002. Carbon-oxygen isotope and trace element constraints on how fluids percolate faulted limestones from the San Andreas Fault system: partitioning of fluid sources and pathways. Chemical Geology 190, 231–250.
Pizzino, L., Quattrocchi, F., Cinti, D., Galli, G., 2004. Fluid geochemistry along the Eliki and Aigion seismogenic segments (Gulf of Corinth, Greece). Comptes Rendus Geosciences 336, 367–374.
Reynolds, R.C., 1985. NEWMOD: A Computer Program for the Calculation of One-Dimensional Diffraction Patterns of Mixed Layer Clays.
Reynolds, R.C., Walker, J.R., 1993. Computer Applications of X-ray Powder Diffraction Analysis of Clay Minerals. Clay Mineral Society Workshop Lectures 5.
Rice, J.R., 2006. Heating and weakening of faults during earthquake slip. Journal of Geophysical Research 111, doi:10.1029/2005JB004006.
Rigo, A., Lyon-Caen, H., Armijo, H.R., Deschamps, A., Hatzfeld, D., Makropoulos, K., Papadimitriou, P., Kassaras, I., 1996. A microseismic study in the western part of the Gulf of Corinth (Greece): implications for large scale normal faulting mechanisms. Geophysical Journal International 126, 663–688.
Roberts, G., Koukouvelas, I.K., 1996. Structural and seismological segmentation of the Gulf of Corinth fault system: implications for models of fault growth. Annali di Geophysica 23, 619–646.
Sachpazi, M., Galvé, A., Laigle, M., Hirn, A., Sokos, E., Serpetsidaki, A., Marthelot, J.-M., Pi Alperin, J.M., Zelt, B., Taylor, B., 2007. Moho topography under central Greece and its compensation by Pn time-terms for the accurate location of hypocenters: the example of the Gulf of Corinth 1995 Aigion earthquake. Tectonophysics 440, 53–65.
Segall, P., Rice, J.R., 1995. Dilatancy, compaction, and slip instability of a fluid saturated fault. Journal of Geophysical Research 100, 22155–22171.
Segall, P., Rice, J.R., 2006. Does shear heating of pore fluid contribute to earthquake nucleation? Journal of Geophysical Research 111, doi:10.1029/2005JB004129.
Shipton, Z.K., Cowie, P.A., 2001. Damage zone and slip-surface evolution over Am to km scales in high-porosity Navajo sandstone, Utah. Journal of Structural Geology 23, 1825–1844.
Sibson, R.H., 1990. Conditions for fault-valve behaviour. In: Knipe, R.J., Rutter, E.H. (Eds.), Deformation Mechanisms, Rheology and Tectonics. Geological Society, London, Special Publications, vol. 54, pp. 15–28.
Sibson, R.H., 1996. Structural permeability of fluid-driven fault-fracture meshes. Journal of Structural Geology 18, 1031–1042.
Sibson, R.H., 2000. Fluid involvement in normal faulting. Journal of Geodynamics 29, 469–499.
Sibson, R.H., 2007. An episode of fault-valve behaviour during compressional inversion? – The 2004 MJ6.8 Mid-Niigata Prefecture, Japan, earthquake sequence. Earth and Planetary Science Letters 257, 188–199.
Srodon, J., Eberl, D., 1984. Illite. In: Baily, S.W. (Ed.), Micas. Reviews in Mineralogy, vol. 13. Mineral. Soc. America, Washington, DC, pp. 495–544.
Sulem, J., Vardoulakis, I., Ouffroukh, H., Perdikatsis, V., 2005. Thermo- Poro-Mechanical properties of the Aigion Fault clayey gouge – application to the analysis of sehar heating and fluid pressurization. Soils and Foundations 45, 97–108.
Sulem, J., Lazar, P., Vardoulakis, I., 2007. Thermo-poro-mechanical properties of clayey gouge and application to rapid fault shearing. International Journal for Numerical and Analytical Methods in Geomechanics 31, 523–540.
Tanaka, H., Chester, F.M., Mori, J.J., Wang, C.-Y., 2007. Drilling into fault zones. Tectonophysics 443, 123–125.
Tessier, D., Dardaine, M., Beaumont, A., Jaunet, A.M., 1998. Swelling pressure and microstructure of an activated swelling clay with temperature. Clay Minerals 33, 255–267.
Tsang, C.-F., Neretnieks, I., 1998. Flow channeling in heterogeneous fractured rocks. Reviews of Geophysics 36, 275–298.
Utada, M., 1980. Hydrothermal alteration related to igneous acidity in Cretaceous and Neogene formations of Japan. Mining Geology Japanese Special 8, 67–83.
Warr, L.N., Cox, S., 2001. Clay mineral transformation and weakening mechanisms along the Alpine Fault, New Zealand. In: Holdsworth, R.E., Strachan, R.A., Magloughlin, J.F., Knipe, R.J. (Eds.), The Nature and Tectonic Significance of Fault Zone Weakening. Geological Society, London, Special Publications, vol. 186, pp. 85–101.
Westaway, R., 2007. Improved modelling of the Quaternary evolution of the Gulf of Corinth, incorporating erosion and sedimentation coupled by lower-crustal flow. Tectonophysics 440, 67–84.
Xypolias, P., Doutsos, T., 2000. Kinematics of rock flow in a crustal-scale shear zone: implication for the orogenic evolution of the southwestern Hellenides. Geological Magazine 137, 81–96.
Zahradník, J., Janský, J., Sokos, E., Serpetsidaki, A., Lyon-Caen, H., Papadimitriou, P., 2004. Modeling the M_L4.7 mainshock of the February–July 2001 earthquake sequence in Aegion, Greece. Journal of Seismology 8, 247–257.
Zoback, M., Harjes, H.-P., 1997. Injection induced earthquakes and the crustal stress at 9 km depth at the KTB deep drilling site, Germany. Journal of Geophysical Research 102, 18477–18492.
Zygouri, V., Verroios, S., Kokkalas, S., Xypolias, P., Koukouvelas, I.K., 2008. Scaling properties within the Gulf of Corinth, Greece; comparison between offshore and onshore active faults. Tectonophysics 453, 193–210.